Transport in Porous Media **55:** 47–70, 2004.

Analytical Solution to the Riemann Problem of Three-Phase Flow in Porous Media

RUBEN JUANES[1] and TADEUSZ W. PATZEK[2,3,*]
[1] *Department of Petroleum Engineering, Stanford University, Stanford, CA 94305, U.S.A.*
[2] *Department of Civil and Environmental Engineering, University of California, Berkeley, CA 94720, U.S.A.*
[3] *Lawrence Berkeley National Laboratory, Earth Sciences Division, Berkeley, CA 94720, U.S.A.*

(Received: 1 October 2002; in final form: 15 July 2003)

Abstract. In this paper we study one-dimensional three-phase flow through porous media of immiscible, incompressible fluids. The model uses the common multiphase flow extension of Darcy's equation, and does not include gravity and capillarity effects. Under these conditions, the mathematical problem reduces to a 2×2 system of conservation laws whose essential features are: (1) the system is strictly hyperbolic; (2) both characteristic fields are nongenuinely nonlinear, with single, connected inflection loci. These properties, which are natural extensions of the two-phase flow model, ensure that the solution is physically sensible. We present the complete analytical solution to the Riemann problem (constant initial and injected states) in detail, and describe the characteristic waves that may arise, concluding that only nine combinations of rarefactions, shocks and rarefaction-shocks are possible. We demonstrate that assuming the saturation paths of the solution are straight lines may result in inaccurate predictions for some realistic systems. Efficient algorithms for computing the exact solution are also given, making the analytical developments presented here readily applicable to interpretation of lab displacement experiments, and implementation of streamline simulators.

Key words: three-phase flow, conservation laws, Buckley–Leverett, hyperbolic system, waves, entropy solution.

1. Introduction

Quantitative predictions of the flow of three immiscible fluids – water, oil and gas – are required to assess many processes of great practical interest: primary oil production below bubble point and with movable water; waterfloods, man-made and natural; immiscible CO_2 floods; steam floods; gravity drainage of gas caps with oil and water; water-alternating-gas (WAG) processes; and contaminant intrusions into the shallow subsurface, just to name a few.

Here we study the classical formulation of three-phase flow, which makes use of the common multiphase extension of Darcy's equation (Muskat, 1949). When the fractional flow approach is used, flow of three immiscible incompressible fluids is described by a pressure equation, and a 2×2 system of saturation equations

*Author for correspondence: e-mail: patzek@patzek.berkeley.edu

(Chavent and Jaffré, 1986). Capillarity effects enter the formulation as a nonlinear diffusion term. The first studies on the mathematical character of the *capillarity-free* system date back to Charny (1963). This work points out the possibility of the system being of mixed elliptic/hyperbolic type. It is concluded, however, that for physically realistic three-phase flows, the system is hyperbolic (Stklyanin, 1960). Bell *et al*. (1986) showed that, for certain relative permeability functions (Stone, 1970), the system is not everywhere hyperbolic. In fact, most relative permeability models used today give rise to systems which are not strictly hyperbolic for the entire range of admissible saturations (Fayers, 1987; Shearer and Trangenstein, 1989; Holden, 1990; Hicks Jr. and Grader, 1996). Loss of strict hyperbolicity typically occurs in bounded regions of the saturation triangle (the so-called elliptic regions), where the system is elliptic in character. The only relative permeability models in the existing literature which do not produce elliptic regions are those where the relative permeability of a phase depends solely on the saturation of that phase (Trangenstein, 1989). This behavior is not supported by experimental results (Oak *et al*., 1990) and pore-scale models (Al-Futaisi and Patzek, 2003). For models of this type, the elliptic region (where eigenvalues are complex conjugates) shrinks to an isolated umbilic point (a saturation state with a real double eigenvalue), thus rendering a *nonstrictly* hyperbolic system at that point. The literature on mixed elliptic/hyperbolic systems and nonstrictly hyperbolic systems is vast (see, e.g., Keyfitz and Shearer, 1990; Lindquist, 1989; Marchesin and Plohr, 2001, and the references therein), yet a complete theory is still lacking.

In our opinion, the presence of elliptic regions contradicts the expected physical behavior of a three-phase displacement (Juanes and Patzek, 2002; Juanes, 2003). They appear as a consequence of using Muskat's extension of Darcy's equation, and common relative permeability functions. Since a Darcy-type formulation does not account for the full physics of multiphase flow, relative permeabilities should be understood as *functionals*, rather than fixed functions of saturations alone. Indeed, it is possible to impose conditions on the relative permeabilities so that the system of saturation equations is strictly hyperbolic inside the saturation triangle (Juanes and Patzek, 2002). These conditions are in agreement with pore-scale physics and experimental data.

Application of the fractional flow theory to multiphase, multicomponent flow was presented by Pope (1980) and Helfferich (1981) for the case of *linear* relative permeability functions, exploiting the analogy with multicomponent chromatography (Helfferich and Klein, 1970; Rhee *et al*., 1989). Extensions of the theory, confined to the case where each relative permeability is a function of its own phase saturation, and for particular initial and injected states, have been presented by Stklyanin (1960), Shalimov (1972), Falls and Schulte (1992a, b), and Marchesin and Plohr (2001), among others. Of particular relevance are the developments of Guzmán and Fayers (1997a, b). They constructed analytical solutions to the Riemann problem of three-phase flow, with and without gravity, and using different classical relative permeability models. In their

work, however, only generic guidelines for the construction of solutions are given.

With the above considerations in mind, we study in this paper the solution to the Riemann problem – initial data given by two constant states separated by a single discontinuity – of three-phase flow. Because the system is strictly hyperbolic for all saturation paths of interest, we use the theory of Lax (1957), as extended by Liu (1974) to systems whose characteristic fields are neither genuinely nonlinear nor linearly degenerate. Although the theory is well known, and has been used profusely, a complete catalogue of solutions to the Riemann problem is not yet available. We use a recent result by Ancona and Marson (2001) to limit the admissible wave structure that may arise in three-phase displacements. Identification of the admissible wave types allows us to present the *complete* catalogue of solutions to the Riemann problem of three-phase flow. Particular attention is given to the actual calculation of the analytical solution. Efficient algorithms are presented, which are based on a predictor–corrector strategy coupled with full Newton iteration, and achieve quadratic convergence in all cases.

In Section 2, we present the governing equations of three-phase flow under the Buckley–Leverett conditions, and the mathematical character of the system is discussed. In Section 3, we present the complete set of solutions to the Riemann problem of three-phase flow. As an application of the analytical solution, in Section 4 we describe an example of water and gas injection into a medium that is initially filled with oil and water, and we evaluate the accuracy of a common approximation of the exact solution. The main conclusions are summarized in Section 5. Algorithms for the efficient calculation of wave curves and selected solution types are compiled in Appendices A and B.

2. Mathematical Model

2.1. GOVERNING EQUATIONS

We study three-phase flow in porous media under the following assumptions: (1) one-dimensional flow; (2) immiscible fluids; (3) incompressible fluids; (4) homogeneous rigid porous medium; (5) multiphase flow extension of Darcy's law; (6) negligible mass forces including gravitational effects; (7) negligible capillary pressure effects; and (8) negligible nonequilibrium effects. When the fractional flow formalism is used, the governing equations are a *pressure* equation, and a 2×2 system of *saturation* equations. The derivation is standard and will be omitted here (Chavent and Jaffré, 1986).

The *pressure equation* reads:

$$\partial_x v_T = 0, \quad 0 < x < L, \ \ t > 0, \tag{1}$$

where $v_T := -(k/\phi)\lambda_T \partial_x p$ is the total velocity, ϕ is the porosity, k is the absolute permeability, and λ_T is the total mobility. The total mobility is the sum of the phase

relative mobilities $\lambda_\alpha := k_{r\alpha}/\mu_\alpha$, where $k_{r\alpha}$ and μ_α are the relative permeability and the dynamic viscosity of the α-phase, respectively. It is also convenient to define the fractional flow function of the α-phase which, when gravity and capillary forces are not considered, is simply $f_\alpha = \lambda_\alpha/\lambda_\mathrm{T}$. Equation (1) dictates that the total velocity v_T is at most a function of time. A nonzero total velocity requires that a pressure difference be imposed at the boundaries.

The *system of saturation equations* is

$$\partial_t \begin{pmatrix} S_\mathrm{w} \\ S_\mathrm{g} \end{pmatrix} + v_\mathrm{T} \partial_x \begin{pmatrix} f_\mathrm{w} \\ f_\mathrm{g} \end{pmatrix} = \begin{pmatrix} 0 \\ 0 \end{pmatrix}, \tag{2}$$

where S_w and S_g are the water and gas saturations, respectively. The solution is restricted to lie in the *saturation triangle*:

$$\mathcal{T} := \{(S_\mathrm{w}, S_\mathrm{g}) : S_\mathrm{w} \geqslant 0, \quad S_\mathrm{g} \geqslant 0, \quad S_\mathrm{w} + S_\mathrm{g} \leqslant 1\}. \tag{3}$$

The saturation triangle is usually depicted as a ternary diagram, on which the pair $(S_\mathrm{w}, S_\mathrm{g})$ is represented as the triple $(S_\mathrm{w}, S_\mathrm{g}, S_\mathrm{o})$, where the oil saturation satisfies $S_\mathrm{o} \equiv 1 - S_\mathrm{w} - S_\mathrm{g}$. We use the equivalent vector notation:

$$\boldsymbol{u} := \begin{pmatrix} u \\ v \end{pmatrix} \equiv \begin{pmatrix} S_\mathrm{w} \\ S_\mathrm{g} \end{pmatrix}, \qquad \boldsymbol{f} := \begin{pmatrix} f \\ g \end{pmatrix} \equiv \begin{pmatrix} f_\mathrm{w} \\ f_\mathrm{g} \end{pmatrix}, \tag{4}$$

and introduce the dimensionless space and time coordinates:

$$x_D := \frac{x}{L}, \qquad t_D := \frac{1}{L} \int_0^t v_\mathrm{T}(\bar{t})\, \mathrm{d}\bar{t}. \tag{5}$$

Understanding the space and time variables as their dimensionless counterparts, the system (2) can be written in its final form:

$$\partial_t \boldsymbol{u} + \partial_x \boldsymbol{f} = \boldsymbol{0}. \tag{6}$$

After a change of variables, the vector of unknowns $\boldsymbol{u}$ may be understood as the vector of *reduced* saturations, rather than *actual* saturations (Juanes and Patzek, 2002; Juanes, 2003). After this renormalization, the three-phase flow region – where all three phases are mobile – covers the entire saturation triangle.

2.2. MATHEMATICAL STRUCTURE OF THE EQUATIONS

If we neglect the dependence of phase viscosities μ_α on pressure and temperature, and take them as constants, the character of the system of saturation equations is a *direct consequence* of the relative permeability model. We understand relative permeabilities as *functionals* of the various system descriptors, rather than *fixed functions* of saturations alone. For the model studied here, they should depend on the viscosity ratios and the saturation history. Therefore, we express the

relative permeabilities as functions of fluid saturations, but assume that an appropriate functional form is used, that is consistent with the fluid, rock, and process descriptors.

The mathematical character of the system (6) is determined by the eigenvalue problem (Zauderer, 1983):

$$\boldsymbol{A}\boldsymbol{r} = \nu\boldsymbol{r}, \tag{7}$$

where

$$\boldsymbol{A} := \mathrm{D}_{\boldsymbol{u}}\boldsymbol{f} \equiv \boldsymbol{f}' \equiv \begin{pmatrix} f_{,u} & f_{,v} \\ g_{,u} & g_{,v} \end{pmatrix} \tag{8}$$

is the Jacobian matrix of the system, ν is an eigenvalue, and $\boldsymbol{r}$ is a right eigenvector, all evaluated at the saturation state $\boldsymbol{u}$. Subscripts after a comma denote differentiation (e.g. $f_{,u} \equiv \partial_u f$). The system is *strictly hyperbolic* if the eigenvalue problem has two real, distinct, eigenvalues. In this case, the Jacobian matrix is diagonalizable and there are two real and linearly independent eigenvectors. In Juanes and Patzek (2002) and Juanes (2003), we show it is possible to formulate relative permeability models that yield a strictly hyperbolic system inside the three-phase flow region. Here, as an example, we use the following relative mobilities:

$$\lambda_{\mathrm{w}} = \left(\frac{1}{\mu_{\mathrm{w}}}\right) u^2, \tag{9}$$

$$\lambda_{\mathrm{g}} = \left(\frac{1}{\mu_{\mathrm{g}}}\right) (\beta_{\mathrm{g}} v + (1-\beta_{\mathrm{g}}) v^2), \quad \beta_{\mathrm{g}} > 0, \tag{10}$$

$$\lambda_{\mathrm{o}} = \left(\frac{1}{\mu_{\mathrm{o}}}\right) (1-u-v)(1-u)(1-v). \tag{11}$$

The most important feature of the model is the positive derivative β_{g} of the gas relative permeability function as it approaches zero. The model considers that the relative permeabilities of the most and least wetting fluids (usually water and gas) depend only on their own saturation, whereas the relative permeability of the intermediate wetting fluid (usually oil) depends on all saturations. This is a common assumption in hydrogeology (Parker *et al.*, 1987) and petroleum engineering (Charny, 1963; Stone, 1970, 1973). Although we do *not* defend this assumption in general, it can be shown (Juanes, 2003) that the relative mobilities (9)–(11) yield a system which is strictly hyperbolic everywhere in the saturation triangle, as long as the following conditions are satisfied:

$$\beta_{\mathrm{g}} > \frac{\mu_{\mathrm{g}}}{\sqrt{\mu_{\mathrm{o}}\mu_{\mathrm{w}}}}, \quad \mu_{\mathrm{w}} < 2\mu_{\mathrm{o}}. \tag{12}$$

For illustrative purposes, we take reasonable values of the viscosities:

$$\mu_{\mathrm{w}} = 0.875, \qquad \mu_{\mathrm{g}} = 0.03, \qquad \mu_{\mathrm{o}} = 2\,\mathrm{cp}, \tag{13}$$

and a small value of the endpoint slope: $\beta_g = 0.1$. These values of the parameters satisfy the two conditions (12).

3. Solution to the Riemann Problem

The Riemann problem consists in finding a (usually weak) solution to the system of conservation laws:

$$\partial_t \boldsymbol{u} + \partial_x \boldsymbol{f} = \boldsymbol{0}, \quad -\infty < x < \infty, \ \ t > 0, \tag{14}$$

with initial condition

$$\boldsymbol{u}(x,0) = \begin{cases} \boldsymbol{u}_l & \text{if } x < 0, \\ \boldsymbol{u}_r & \text{if } x > 0. \end{cases} \tag{15}$$

Equation (14) is an idealization, in which it is assumed that the solution is not affected by the outlet boundary conditions ($x = L$). The conditions at the boundary determine, however, the overall pressure gradient and, in turn, the total velocity v_T. The imposed total velocity enters the formulation through the dimensionless time defined in Equation (5). The solution to the Riemann problem is extremely valuable for practical applications. Laboratory experiments often reproduce the conditions of the Riemann problem. The solution to the Riemann problem gives information about the structure of the system of equations, and can be used as the building block for obtaining solutions to problems with more complex initial conditions, such as in the Godunov method (LeVeque, 1992). Analytical solutions to the Riemann problem are also valuable in the context of streamline simulation (Batycky *et al.*, 1997).

The system of conservation laws (6) describing three-phase flow is a 2×2 system, which is strictly hyperbolic for all saturation paths of interest (Juanes and Patzek, 2002). The theory of strictly hyperbolic systems was compiled by Lax (1957), for systems whose characteristic fields are either genuinely nonlinear or linearly degenerate. The theory of Lax was extended by Liu (1974) to find Riemann solutions for systems with nongenuinely nonlinear fields. This well-known theory will be used here to describe the admissible wave structure, and the complete set of solutions, to the Riemann problem of three-phase flow.

The problem described by Equations (14)–(15) is invariant under uniform stretching of coordinates $(x,t) \mapsto (cx, ct)$. Therefore, we seek a self-similar solution of the form

$$\boldsymbol{u}(x,t) = \boldsymbol{U}(\zeta), \tag{16}$$

where the similarity variable is simply $\zeta := x/t$. Because the system under consideration is strictly hyperbolic, the solution to the Riemann problem comprises two separated waves, $\mathcal{W}_1$ (slow wave) and $\mathcal{W}_2$ (fast wave), connecting three constant states, $\boldsymbol{u}_l$ (left), $\boldsymbol{u}_m$ (middle) and $\boldsymbol{u}_r$ (right):

$$\boldsymbol{u}_l \xrightarrow{\mathcal{W}_1} \boldsymbol{u}_m \xrightarrow{\mathcal{W}_2} \boldsymbol{u}_r. \tag{17}$$

3.1. WAVE STRUCTURE

From the theory of strictly hyperbolic conservation laws, a wave of the i-family consists of i-rarefactions, i-shocks and/or i-contact discontinuities.

3.1.1. *Integral Curves and Rarefactions*

An *i-rarefaction* is a smooth function $\boldsymbol{U}_i(\zeta)$ satisfying the eigenvalue problem

$$\boldsymbol{A}(\boldsymbol{U})\boldsymbol{U}' = \zeta \boldsymbol{U}', \tag{18}$$

where the parameter ζ is not arbitrary, but the i-eigenvalue of $\boldsymbol{A}(\boldsymbol{U})$. Therefore, an i-rarefaction curve must lie on an *integral curve* of the i-family, that is, a curve whose tangent at any point $\boldsymbol{U}$ is in the direction of the i-eigenvector $\boldsymbol{r}_i(\boldsymbol{U})$ at that point. The two families of integral curves are depicted in Figure 1 for the relative mobilities (9)–(11). A rarefaction curve $\boldsymbol{U}_i(\zeta)$ is admissible only if the characteristic speed v_i increases *monotonically* along the curve from the left state to the right state. Rarefaction curves can be calculated by simple numerical integration with a Runge–Kutta algorithm, as explained in Appendix A.1.

3.1.2. *Hugoniot Loci and Shocks*

A *shock* is a traveling discontinuity. Any propagating discontinuity connecting two states, $\boldsymbol{u}_-$ and $\boldsymbol{u}_+$, must satisfy the *Rankine–Hugoniot jump condition* (LeVeque, 1992):

$$\boldsymbol{f}(\boldsymbol{u}_+) - \boldsymbol{f}(\boldsymbol{u}_-) = \sigma(\boldsymbol{u}_+; \boldsymbol{u}_-) \cdot (\boldsymbol{u}_+ - \boldsymbol{u}_-), \tag{19}$$

where $\sigma(\boldsymbol{u}_+; \boldsymbol{u}_-)$ is the speed of propagation of the discontinuity. For a fixed state $\boldsymbol{u}_-$, the *Hugoniot locus* is the set of states $\boldsymbol{u}_+$ which can be connected to $\boldsymbol{u}_-$ such that Equation (19) is satisfied. There are two families of solutions, $\mathcal{H}_1(\boldsymbol{u}_-)$ and $\mathcal{H}_2(\boldsymbol{u}_-)$, one for each characteristic family. Hugoniot curves are tangent to the

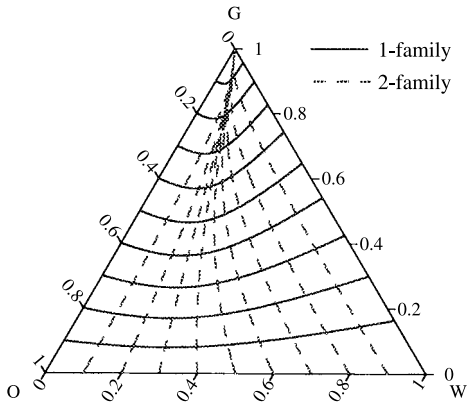

Figure 1. Integral curves for the relative mobilities (9)–(11).

corresponding eigenvectors at the reference point $\boldsymbol{u}_-$, but *do not* coincide with integral curves (LeVeque, 1992).

A genuine shock of the i-family (an i-shock) is physically admissible if it satisfies the *Lax entropy condition* (Lax, 1957):

$$v_i(\boldsymbol{u}_-) > \sigma_i(\boldsymbol{u}_+; \boldsymbol{u}_-) > v_i(\boldsymbol{u}_+), \tag{20}$$

which implies that characteristics of the i-family go *into* the shock. A shock curve of the i-family passing through point $\boldsymbol{u}_-$, denoted as $\mathcal{S}_i(\boldsymbol{u}_-)$, corresponds to a subset of the Hugoniot locus $\mathcal{H}_i(\boldsymbol{u}_-)$, for which the entropy condition (20) is satisfied. An algorithmic procedure for the calculation of the Hugoniot loci, based on a Newton iterative scheme, is detailed in Appendix A.2.

3.1.3. *Inflection Loci and Rarefaction–Shocks*

The notion of genuine nonlinearity is central to the wave structure arising in multiphase flow. The i-field is said to be *genuinely nonlinear* if the i-eigenvalue v_i varies monotonically along integral curves of the i-family. This condition is equivalent to that of convexity of the flux function for scalar conservation laws. However, the characteristic fields of the system describing three-phase flow are not genuinely nonlinear: eigenvalues attain local maxima along integral curves. The *inflection locus* $\mathcal{V}_i$ for the i-characteristic field is the set of points $\boldsymbol{U}$ such that

$$\nabla v_i(\boldsymbol{U}) \cdot \boldsymbol{r}_i(\boldsymbol{U}) = 0, \tag{21}$$

that is, the locations at which v_i attain either a maximum or a minimum value when moving along integral curves of the i-family. In Figure 2 we show contour plots of eigenvalues and the inflection loci for both characteristic families. The inflection locus of each characteristic family is a single connected curve, which corresponds to *maxima* of eigenvalues. This is consistent with the well-known behavior in the

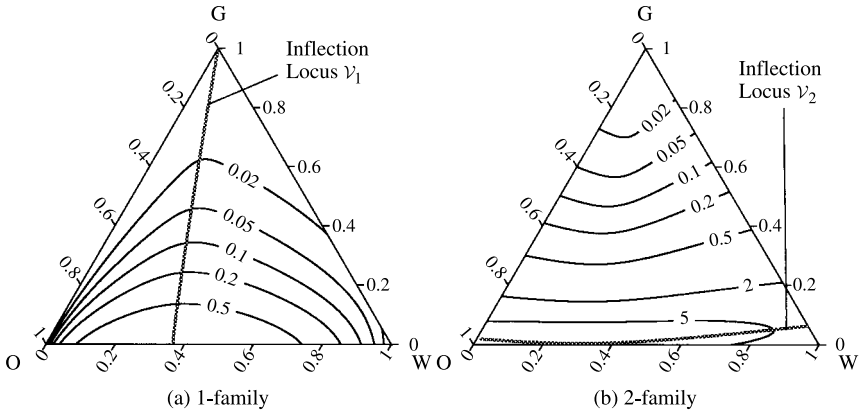

Figure 2. Contour plots of eigenvalues v_i and the inflection loci $\mathcal{V}_i$ of both characteristic families, for the relative mobilities (9)–(11).

two-phase flow case, for which the fractional flow function is S-shaped, and the inflection point corresponds to the *maximum value* of the derivative.

For a strictly hyperbolic system whose characteristic fields are not genuinely nonlinear, each wave may consist in a combination of rarefactions and discontinuities (Liu, 1974). In our case, since the inflection locus for each field is a single connected curve satisfying certain orthogonality conditions with respect to integral curves, the composite wave has at most one rarefaction and one discontinuity. Moreover, because the inflection loci correspond to local *maxima* of eigenvalues along integral curves, the rarefaction is always slower than the shock (Ancona and Marson, 2001).

A *rarefaction–shock* of the i-family connecting the left and right states $\boldsymbol{u}_{\mathrm{l}}$ and $\boldsymbol{u}_{\mathrm{r}}$, $\mathcal{R}_i\mathcal{S}_i(\boldsymbol{u}_{\mathrm{l}}, \boldsymbol{u}_{\mathrm{r}})$, is a curve consisting of an i-rarefaction curve emanating from $\boldsymbol{u}_{\mathrm{l}}$, connected at some intermediate point $\boldsymbol{u}_*$ to an i-shock curve, which ends at the right state. At the post-shock state $\boldsymbol{u}_*$, the following property holds:

$$\nu_i(\boldsymbol{u}_*) = \sigma_i(\boldsymbol{u}_{\mathrm{r}}; \boldsymbol{u}_*). \tag{22}$$

The solution may involve an i-rarefaction–shock only if the left and right states lie on opposite sides with respect to the inflection locus $\mathcal{V}_i$.

Any discontinuity in the i-wave, connecting two states $\boldsymbol{u}_-$ (left) and $\boldsymbol{u}_+$ (right), must satisfy the Liu entropy condition (Liu, 1974):

$$\sigma_i(\boldsymbol{u}_+; \boldsymbol{u}_-) \leqslant \sigma_i(\boldsymbol{u}; \boldsymbol{u}_-), \tag{23}$$

for all states $\boldsymbol{u} \in \mathcal{S}_i(\boldsymbol{u}_-)$ between $\boldsymbol{u}_-$ and $\boldsymbol{u}_+$. In the particular case of three-phase flow, where inflection loci are single connected curves corresponding to maxima of eigenvalues, it can be shown (Ancona and Marson, 2001) that condition (23) is equivalent to the following simpler condition:

$$\nu_i(\boldsymbol{u}_-) \geqslant \sigma_i(\boldsymbol{u}_+; \boldsymbol{u}_-) > \nu_i(\boldsymbol{u}_+). \tag{24}$$

Algorithms for calculating rarefaction–shock curves, which are based on a predictor–corrector strategy, are given in Appendix A.3.

3.2. COMPLETE SET OF SOLUTIONS

The analysis of the wave structure dictates that a wave of the i-family connecting two constant states may only be one of the following: an i-rarefaction ($\mathcal{R}_i$), an i-shock ($\mathcal{S}_i$), or an i-rarefaction–shock ($\mathcal{R}_i\mathcal{S}_i$). Since the full solution to the Riemann problem is a sequence of two waves, $\mathcal{W}_1$ and $\mathcal{W}_2$, there are *only* nine possible combinations of solutions. In Figure 3 we plot representative saturation paths in the ternary diagram for all nine solution types. Inflection loci (dash-dotted curves) are plotted for reference also. These different cases provide the *complete set of solutions* to the Riemann problem of three-phase flow, when the following physical properties are satisfied: (1) the system is strictly hyperbolic; and (2) the

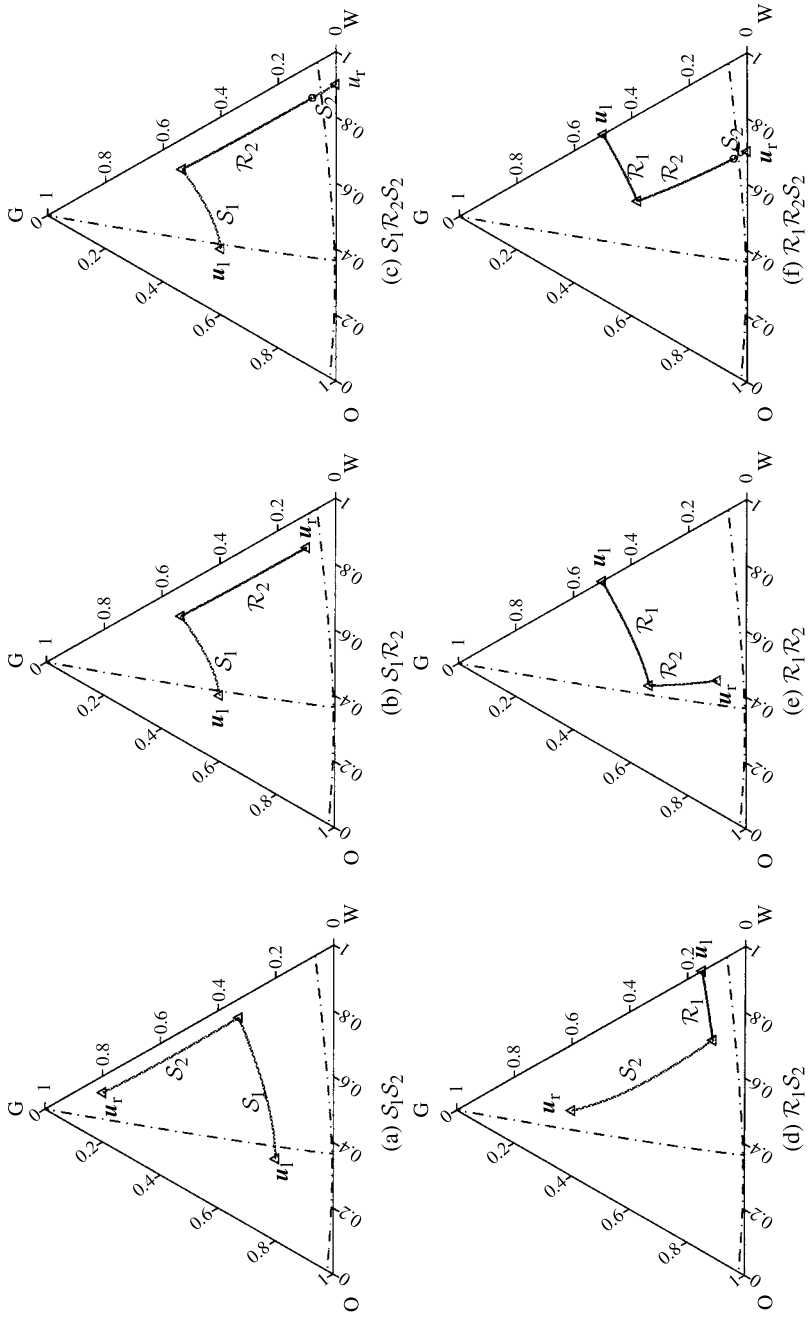

Figure 3. Examples of the saturation paths for all nine solution types.

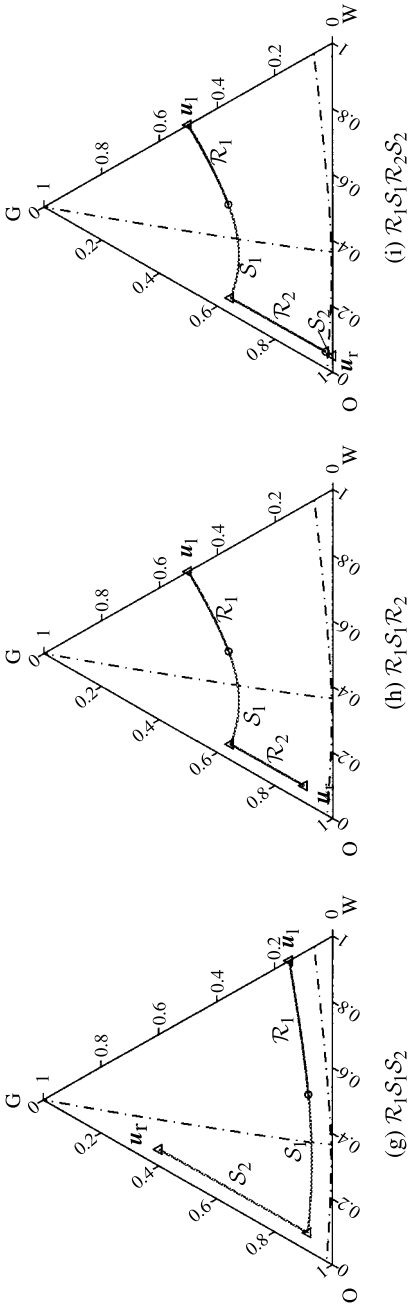

(g) $\mathcal{R}_1\mathcal{S}_1\mathcal{S}_2$ (h) $\mathcal{R}_1\mathcal{S}_1\mathcal{R}_2$ (i) $\mathcal{R}_1\mathcal{S}_1\mathcal{R}_2\mathcal{S}_2$

Figure 3. (continued)

inflection loci are single connected curves, transversal to the integral curves, and correspond to maxima of the eigenvalues. Efficient algorithms for the complete calculations of the solution are given in Appendix B. They are based on a predictor–corrector strategy coupled with a full Newton iteration, which achieves quadratic convergence in all cases.

4. Application Example: Water–Gas Injection

The importance of three-phase flow in gas and water-alternating-gas injection processes at the reservoir scale has been pointed out by Guzmán *et al*. (1994). In this section we illustrate the applicability of the theory presented in Section 3, to develop exact solutions for a water–gas injection problem.

The problem involves simultaneous injection of water and gas into a medium that is initially filled with oil and water. This physical problem is modeled mathematically as a Riemann problem, where the left (injected) saturation state is $\boldsymbol{u}_{\mathrm{l}} = (0.5, 0.5)$, and the right (initial) saturation state is $\boldsymbol{u}_{\mathrm{r}} = (0.05, 0)$. We use the relative mobilities in Equations (9)–(11) with $\beta_{\mathrm{g}} = 0.1$, and the fluid viscosities in (13).

4.1. EXACT SOLUTION

The exact solution is of type $\mathcal{R}_1\mathcal{S}_1\mathcal{R}_2\mathcal{S}_2$, that is, both the slow and fast waves are rarefaction–shocks. The variables that fully characterize the solution are: the intermediate constant state $\boldsymbol{u}_{\mathrm{m}}$, the shock speeds σ_1 and σ_2, and the post-shock states $\boldsymbol{u}_1^*$ and $\boldsymbol{u}_2^*$ of each wave. Schematically, the solution is represented as follows:

$$\boldsymbol{u}_{\mathrm{l}} \xrightarrow{\mathcal{R}_1} \boldsymbol{u}_1^* \xrightarrow{\mathcal{S}_1} \boldsymbol{u}_{\mathrm{m}} \xrightarrow{\mathcal{R}_2} \boldsymbol{u}_2^* \xrightarrow{\mathcal{S}_2} \boldsymbol{u}_{\mathrm{r}}. \tag{25}$$

A detailed algorithm to obtain this solution is given in Appendix B.3.

In Figure 4 we show the saturation path of the exact solution. The corresponding saturation profiles are plotted in Figure 5 against the similarity variable $\zeta = x/t$. Because the characteristic speeds of the slow and fast waves are very different, the entire saturation profile shown on the right plot 5(b) does not allow to visualize the structure of the slow wave (1-wave). A detail of the 1-wave is shown on the left plot 5(a). It is apparent that the 1-wave involves changes in the saturation of *all three* fluids.

4.2. APPROXIMATE SOLUTION

A common approximation of the solution consists in assuming that the saturation paths are straight lines parallel to the edges of the saturation triangle. The physical motivation for this assumption is to split the actual three-phase flow displacement

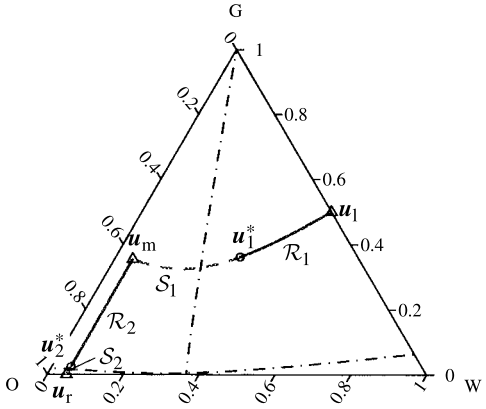

Figure 4. Saturation path of the *exact solution*.

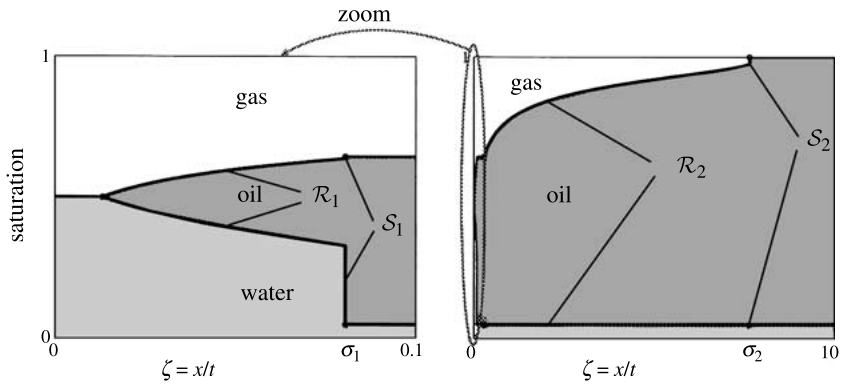

(a) Detail of the 1-wave (b) Entire saturation profile

Figure 5. Saturation profiles of the *exact solution*.

into a sequence of two successive *two-phase* displacements. This approximation, which dates back to the early conceptual model of a waterflood in the presence of gas (Kyte *et al.*, 1956), is equivalent to assuming that the fast wave is a displacement of oil exclusively by gas, and that the slow wave is a displacement of oil exclusively by water. Therefore, it is assumed that the water saturation is constant along the fast wave, and the gas saturation is constant along the slow wave. The immediate benefit of this simplification is that the solution may be computed using the theory of *two-phase* Buckley–Leverett flow. Here we evaluate the accuracy of this simplifying assumption.

In Figure 6 we show the saturation paths that result from the assumption described above. The intermediate constant state $\boldsymbol{u}_m$ is at the intersection of the two wave paths. Each wave is then resolved using classical (two-phase) Buckley–Leverett theory. In this case, the slow wave is a 1-shock, and the fast wave is a 2-rarefaction–shock. In Figure 7 we plot the saturation profiles of the approximate

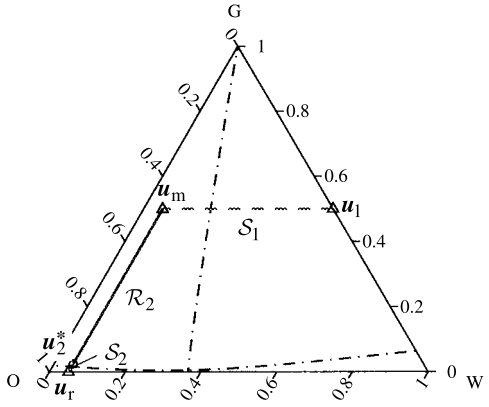

Figure 6. Saturation path of the *approximate solution*.

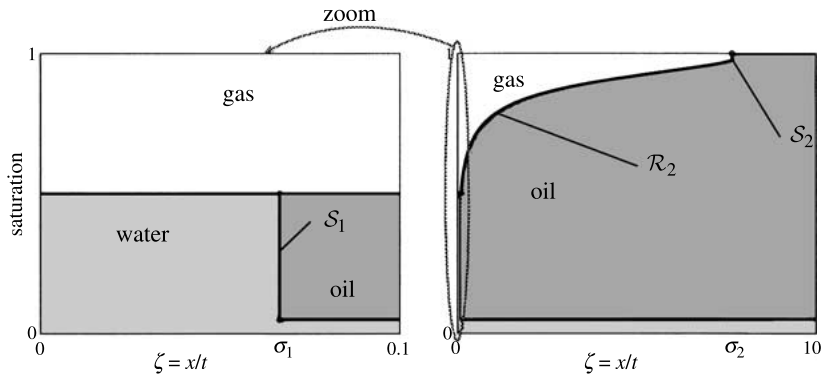

(a) Detail of the 1-wave (b) Entire saturation profile

Figure 7. Saturation profiles of the *approximate solution*.

solution against the similarity variable ζ. The right plot 7(b) shows the entire saturation profile, and the left plot 7(a) a detail of the 1-wave. It is evident that, while the qualitative behavior of the fast wave is similar to that of the exact solution, the structure of the slow wave is very different.

4.3. DISCUSSION

To evaluate better the accuracy of the straight-line approximation of the saturation paths, we compare the oil production of the exact and the approximate solutions. This is done by taking a fixed length L, and calculating the amount of oil displaced at the outlet at any given time. Using the definitions of dimensionless space and time coordinates in Equation (5), we plot the results against the dimensionless time $\tau := 1/\zeta = t/x$. The variables of interest are the *dimensionless oil production rate*

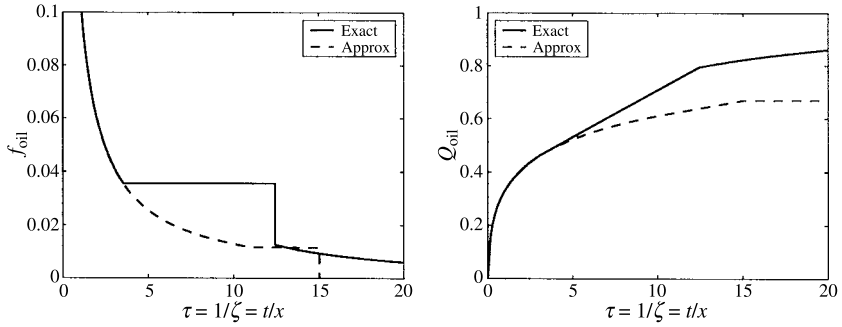

(a) Oil production rate (b) Cumulative oil production

Figure 8. Comparison of the dimensionless oil production rate (left) and cumulative oil production (right), predicted by the exact solution and the approximate solution.

f_{oil} and the *dimensionless cumulative oil production* Q_{oil}:

$$f_{\text{oil}}(\tau) = 1 - f(\tau) - g(\tau), \tag{26}$$

$$Q_{\text{oil}}(\tau) = \int_0^\tau f_{\text{oil}}(\eta)\,\mathrm{d}\eta. \tag{27}$$

In Figure 8(a) we plot the dimensionless oil production rate f_{oil}, as predicted by the exact solution and the approximate solution. The approximate solution agrees well with the exact solution at early times (roughly, for $\tau < 3$) because the exact saturation path of the fast wave may be approximated accurately by a straight line of constant water saturation. However, the approximate solution deviates very significantly from the exact solution for times $\tau > 3$, because both the saturation and the speed of propagation of the oil bank are predicted incorrectly.

The dimensionless *cumulative* oil production Q_{oil}, which is simply the area under the curve in Figure 8(a), is shown in Figure 8(b) for both the exact and the approximate solutions. The curve given by the exact solution tends asymptotically to a value of $Q_{\text{oil,max}} = 0.95$, which is equal to the initial reduced oil saturation. In contrast, the curve predicted by the approximate solution reaches a plateau of $Q_{\text{oil,max}} \approx 0.67$ at time $\tau \approx 15$. This behavior illustrates that the approximate solution is *not* mass conservative.

The results presented above motivate the following *remarks*:

1. Rarefaction–shock waves, common in two-phase displacements, appear also in realistic scenarios of three-phase flow.
2. In the realm of Buckley–Leverett models of three-phase flow, individual waves involve simultaneous three-phase displacements.
3. In general, the saturation paths induced by the exact characteristic waves are *not* straight lines on the ternary diagram. Saturation paths are straight lines only for linear relative permeability functions, or for very particular initial and injected saturation states.

4. Splitting a three-phase displacement into a sequence of two successive *two-phase* displacements is an assumption that is not generally appropriate. In particular, the approximate solution calculated under this assumption does not satisfy an overall mass balance.

5. Conclusions

The key result of this paper is the *complete* general analytical solution to the Riemann problem of three-phase flow of immiscible, incompressible fluids, when gravity and capillarity are not included in the formulation, and under the following physical assumptions: (1) the system is strictly hyperbolic for all saturation paths of interest; (2) the inflection loci are single connected curves, which correspond to maxima of the eigenvalues. The solution comprises two waves separated by an intermediate state of constant saturation. Each of these two waves may only be a rarefaction, a shock, or a rarefaction–shock. Thus, there are only nine combinations of admissible waves. All these combinations, which constitute the complete set of solutions to the Riemann problem, are discussed in our paper. We demonstrate that, in general, a three-phase flow displacement should *not* be approximated by a sequence of two successive two-phase displacements. Such approximation does not satisfy an overall mass balance, and may lead to very inaccurate predictions of oil recovery.

We are currently extending the analytical solution presented here to the case when saturation states are outside the three-phase flow region, that is, when one or more phases are immobile. Capillarity effects, which smear the traveling discontinuities of the capillarity-free solution, may also be incorporated by the method of asymptotic expansions (Barenblatt *et al.*, 1990).

We anticipate that the results of this paper will be relevant to: (1) the interpretation of three-phase displacement experiments; (2) implementation of the solution in streamtube simulators; (3) development of improved relative permeability models; and (4) validation of numerical methods.

Acknowledgements

The authors wish to express their gratitude to Dr Dmitriy B. Silin for his careful revision of the manuscript. We thank Dr A. R. Kacimov for pointing out the book by Charny (1963). The comments of two other anonymous reviewers lead to an improved presentation of the material, and are also appreciated. This work was supported by the Laboratory Directed Research and Development Program of Lawrence Berkeley National Laboratory under the Department of Energy Contract No. DE-AC03-76SF00098. Funding provided by the Barrié de la Maza, Jane Lewis, and Repsol-YPF fellowships, awarded to the first author, is also gratefully acknowledged.

Appendix A. Solution Algorithms for the Wave Curves

A.1. RAREFACTION CURVES

Let $\tilde{\boldsymbol{u}}_i(\xi) = (\tilde{u}_i(\xi), \tilde{v}_i(\xi))$ be a parameterization of an i-rarefaction curve $\mathcal{R}_i(\hat{\boldsymbol{u}})$, starting at the reference state $\hat{\boldsymbol{u}} = (\hat{u}, \hat{v})$. It satisfies the initial value problem:

$$\tilde{\boldsymbol{u}}_i'(\xi) = \alpha(\xi)\boldsymbol{r}_i(\tilde{\boldsymbol{u}}_i(\xi)), \quad \text{with } \tilde{\boldsymbol{u}}_i(0) = \hat{\boldsymbol{u}}, \tag{A.1}$$

where $\alpha(\xi)$ is some scalar factor. For a 1-*rarefaction curve* we choose the parameterization $\tilde{u}_1(\xi) = \hat{u} + \xi$, and the initial value problem (A.1) reduces to

$$\tilde{v}_1'(\xi) = r_{1v}/r_{1u}, \quad \text{with } \tilde{v}_1(0) = \hat{v}. \tag{A.2}$$

A simple Runge–Kutta algorithm can be used to integrate this scalar ordinary differential equation. Integration of the 2-*rarefaction curve* is analogous, using the parameterization $\tilde{v}_2(\xi) = \hat{v} + \xi$.

A.2. SHOCK CURVES

Let $\tilde{\boldsymbol{u}}_i(\xi) = (\tilde{u}_i(\xi), \tilde{v}_i(\xi))$ be a parameterization of an i-shock curve $\mathcal{S}_i(\hat{\boldsymbol{u}})$, starting at the reference state $\hat{\boldsymbol{u}} = (\hat{u}, \hat{v})$. For a 1-*shock curve* we use the parameterization $\tilde{u}_1(\xi) = \hat{u} + \xi$. For each value of the parameter ξ, the shock speed σ_1 and the gas saturation $\tilde{v}_1$ are determined by imposing the Rankine–Hugoniot condition. We use Newton's method to find the solution to the system of nonlinear equations, as indicated in Figure 9.

For the 2-*shock curve* we use the parameterization $\tilde{v}_2(\xi) = \hat{v} + \xi$. The iterative procedure to obtain the solution is identical to that of the 1-shock curve, but now the system needs to be solved for $\tilde{u}_2$ and σ_2. The solution vector, residual vector and Jacobian matrix are

$$\begin{aligned} \boldsymbol{x} &= \begin{pmatrix} \tilde{u}_2 \\ \sigma_2 \end{pmatrix}, \qquad \boldsymbol{R} = \begin{pmatrix} f(\tilde{u}_2, \tilde{v}_2) - f(\hat{u}, \hat{v}) - \sigma_2(\tilde{u}_2 - \hat{u}) \\ g(\tilde{u}_2, \tilde{v}_2) - g(\hat{u}, \hat{v}) - \sigma_2(\tilde{v}_2 - \hat{v}) \end{pmatrix}, \\ \boldsymbol{J} &= \frac{\partial \boldsymbol{R}}{\partial \boldsymbol{x}} = \begin{pmatrix} f_{,u}(\tilde{u}_2, \tilde{v}_2) - \sigma_2 & -(\tilde{u}_2 - \hat{u}) \\ g_{,u}(\tilde{u}_2, \tilde{v}_2) & -(\tilde{v}_2 - \hat{v}) \end{pmatrix}. \end{aligned} \tag{A.3}$$

A.3. RAREFACTION–SHOCK CURVES

To compute rarefaction–shock curves of the 1-*characteristic family*, we assume that the left state $\boldsymbol{u}_1$ and the first component u_r of the right state are known. We need to solve for the second component v_r of the right state, the speed σ_1 of the shock, and the post-shock state $\boldsymbol{u}_*$. These unknowns are obtained using the predictor–corrector algorithm of Figure 10. A schematic of the kth iteration is shown in Figure 11. The $\mathcal{R}_1$ and $\mathcal{S}_1$ curves are connected with second-order tangency (same

1. Set $k = 0$. Initial guess:

$$\boldsymbol{x}^{(0)} = \begin{pmatrix} \sigma_1^{(0)} \\ \tilde{v}_1^{(0)} \end{pmatrix}.$$

2. Evaluate residual vector and Jacobian matrix:

$$\boldsymbol{R}^{(k)} = \begin{pmatrix} f(\tilde{u}_1, \tilde{v}_1^{(k)}) - f(\hat{u}, \hat{v}) - \sigma_1^{(k)}(\tilde{u}_1 - \hat{u}) \\ g(\tilde{u}_1, \tilde{v}_1^{(k)}) - g(\hat{u}, \hat{v}) - \sigma_1^{(k)}(\tilde{v}_1^{(k)} - \hat{v}) \end{pmatrix},$$

$$\boldsymbol{J}^{(k)} = \left.\frac{\partial \boldsymbol{R}}{\partial \boldsymbol{x}}\right|^{(k)} = \begin{pmatrix} -(\tilde{u}_1 - \hat{u}) & f_{,v}(\tilde{u}_1, \tilde{v}_1^{(k)}) \\ -(\tilde{v}_1^{(k)} - \hat{v}) & g_{,v}(\tilde{u}_1, \tilde{v}_1^{(k)}) - \sigma_1^{(k)} \end{pmatrix}.$$

3. Solve linear system for the increment $\delta \boldsymbol{x}^{(k)}$:

$$\boldsymbol{J}^{(k)} \delta \boldsymbol{x}^{(k)} = \boldsymbol{R}^{(k)}.$$

4. Update solution: $\boldsymbol{x}^{(k+1)} = \boldsymbol{x}^{(k)} - \delta \boldsymbol{x}^{(k)}$.

5. Check convergence:

   IF $||\boldsymbol{R}|| < \epsilon$ STOP

   ELSE Set $k \leftarrow k + 1$ and GOTO 2.

Figure 9. Newton algorithm for the 1-shock curve.

1. Set $k = 0$. Initial guess $v_{\mathrm{r}}^{(0)}$.

2. *Predictor:*

   (i) Integrate along rarefaction curve $\mathcal{R}_1(\boldsymbol{u}_{\mathrm{l}})$ as in Equation (29) until

$$\nu_1(\tilde{\boldsymbol{u}}) = \sigma_1(\boldsymbol{u}_{\mathrm{r}}^{(k)}; \tilde{\boldsymbol{u}}) = \frac{f(\boldsymbol{u}_{\mathrm{r}}^{(k)}) - f(\tilde{\boldsymbol{u}})}{u_{\mathrm{r}} - \tilde{u}}.$$

   (ii) Set $\boldsymbol{u}_*^{(k+1)} = \tilde{\boldsymbol{u}}$ at which integration terminated.

3. *Corrector:* Solve for $\sigma_1^{(k+1)}$ and $v_{\mathrm{r}}^{(k+1)}$ by imposing that the right state belongs to the shock curve passing through the post-shock state, $\boldsymbol{u}_{\mathrm{r}}^{(k+1)} \in \mathcal{S}_1(\boldsymbol{u}_*^{(k+1)})$, using the Newton algorithm in Figure 9.

4. Check convergence:

   IF $|v_{\mathrm{r}}^{(k+1)} - v_{\mathrm{r}}^{(k)}| < \epsilon$ STOP

   ELSE Set $k \leftarrow k + 1$ and GOTO 2.

Figure 10. Predictor–corrector algorithm for the 1-rarefaction–shock.

slope and curvature). This property ensures that the predictor–corrector algorithm in Figure 10 will achieve quadratic convergence.

The algorithm to compute a rarefaction–shock of the 2-*characteristic family* is completely analogous. In this case, the left state $\boldsymbol{u}_{\mathrm{l}}$ and the *second* component v_{r} of

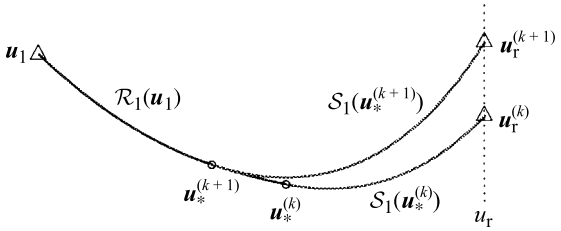

Figure 11. Schematic of the kth iteration of the predictor–corrector algorithm for the 1-rarefaction–shock.

the right state are known, and we use a predictor–corrector algorithm to compute the first component u_r of the right state, the speed σ_2 of the shock, and the post-shock state $\boldsymbol{u}_*$.

B. Solution Algorithms for Selected Solution Types

The solution of the Riemann problem of three-phase flow consists in a sequence of two waves connecting three constant states. The complete set of solutions (nine cases) is given in Section 3.2. In this appendix we describe efficient algorithms for the calculation of selected solution types. Other cases may be computed similarly.

B.1. $\mathcal{S}_1\mathcal{S}_2$ SOLUTION

We consider a solution consisting in two genuine shocks. The unknowns are the intermediate constant state $\boldsymbol{u}_m = (u_m, v_m)$ and the shock speeds σ_1 and σ_2. These four scalar unknowns may be determined by imposing the Rankine–Hugoniot jump condition on each shock. We propose using a full Newton iterative procedure to achieve quadratic convergence. The solution vector $\boldsymbol{x}$, the residual vector $\boldsymbol{R}$ and the Jacobian matrix $\boldsymbol{J}$ are given by

$$\boldsymbol{x} = \begin{pmatrix} \sigma_1 \\ v_m \\ u_m \\ \sigma_2 \end{pmatrix}, \qquad \boldsymbol{R} = \begin{pmatrix} f(u_m, v_m) - f(u_l, v_l) - \sigma_1(u_m - u_l) \\ g(u_m, v_m) - g(u_l, v_l) - \sigma_1(v_m - v_l) \\ f(u_m, v_m) - f(u_r, v_r) - \sigma_2(u_m - u_r) \\ g(u_m, v_m) - g(u_r, v_r) - \sigma_2(v_m - v_r) \end{pmatrix}, \tag{B.1}$$

$$\boldsymbol{J} = \begin{pmatrix} -(u_m - u_l) & f_{,v}(u_m, v_m) & f_{,u}(u_m, v_m) - \sigma_1 & 0 \\ -(v_m - v_l) & g_{,v}(u_m, v_m) - \sigma_1 & g_{,u}(u_m, v_m) & 0 \\ 0 & f_{,v}(u_m, v_m) & f_{,u}(u_m, v_m) - \sigma_2 & -(u_m - u_r) \\ 0 & g_{,v}(u_m, v_m) - \sigma_2 & g_{,u}(u_m, v_m) & -(v_m - v_r) \end{pmatrix}. \tag{B.2}$$

The solution is valid if each wave satisfies the Lax entropy condition:

$$\mathcal{S}_1 : \nu_1(\boldsymbol{u}_l) > \sigma_1 > \nu_1(\boldsymbol{u}_m), \quad \sigma_1 < \nu_2(\boldsymbol{u}_m),$$
$$\mathcal{S}_2 : \nu_2(\boldsymbol{u}_m) > \sigma_2 > \nu_2(\boldsymbol{u}_r), \quad \sigma_2 > \nu_1(\boldsymbol{u}_m).$$

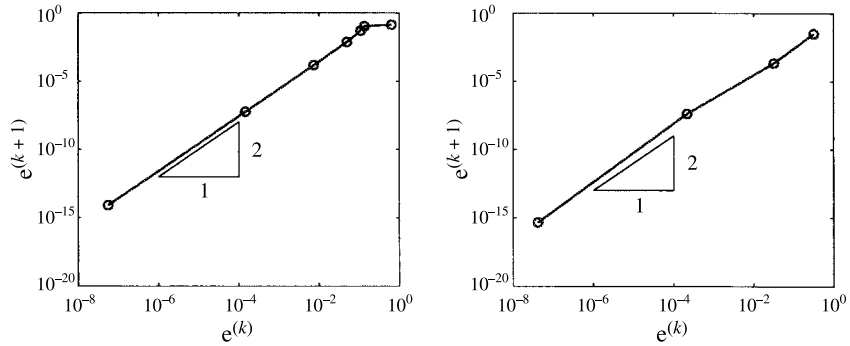

(a) $\mathcal{S}_1\mathcal{S}_2$ solution (b) $\mathcal{R}_1\mathcal{R}_2$ solution

Figure 12. Performance of the Newton iterative scheme for the $\mathcal{S}_1\mathcal{S}_2$ solution (left) and $\mathcal{R}_1\mathcal{R}_2$ solution (right).

As an example, we use the relative mobilities (9)–(11), with the values of fluid viscosities in (13). The left state is $\boldsymbol{u}_\mathrm{l} = (0.25, 0.2)$ and the right state is $\boldsymbol{u}_\mathrm{r} = (0.15, 0.8)$. The schematic of the solution in the ternary diagram is depicted in Figure 3(a). Note that the 1-shock is admissible even though the left and right states of the discontinuity lie on opposite sides of the 1-inflection locus. In Figure 12(a) we show the evolution of the error with the number of iterations of the Newton scheme. The error at iteration k is defined as:

$$\mathrm{e}^{(k)} := \|\delta \boldsymbol{u}_\mathrm{m}^{(k-1)}\|_1 = |u_\mathrm{m}^{(k)} - u_\mathrm{m}^{(k-1)}| + |v_\mathrm{m}^{(k)} - v_\mathrm{m}^{(k-1)}|. \tag{B.3}$$

The rate of convergence of the method is given by the exponent m in the following expression:

$$\mathrm{e}^{(k+1)} \leqslant C(\mathrm{e}^{(k)})^m, \tag{B.4}$$

where C is a bounded positive constant. Plotting $\mathrm{e}^{(k+1)}$ against $\mathrm{e}^{(k)}$ in log–log scale, the convergence rate is simply the asymptotic slope of the curve. Convergence of the iterative procedure is quadratic, as expected.

B.2. $\mathcal{R}_1\mathcal{R}_2$ SOLUTION

We consider the case when both waves are rarefaction waves. By contrast to the previous case, in which the intersecting curves were given by algebraic equations, rarefaction curves are defined by differential equations. We suggest a predictor–corrector strategy to find $\boldsymbol{u}_\mathrm{m}$ iteratively. The algorithm is given in Figure 13, and the kth iteration is illustrated in Figure 14.

The solution is admissible if it is single-valued, that is:

$\mathcal{R}_1 : \nu_1$ increases monotonically along $\mathcal{R}_1$ from $\boldsymbol{u}_\mathrm{l}$ to $\boldsymbol{u}_\mathrm{m}$,

$\mathcal{R}_2 : \nu_2$ increases monotonically along $\mathcal{R}_2$ from $\boldsymbol{u}_\mathrm{m}$ to $\boldsymbol{u}_\mathrm{r}$.

1. Set $k = 0$. Initial guess $\boldsymbol{u}_{\mathrm{m}}^{(0)} = (u_{\mathrm{m}}^{(0)}, v_{\mathrm{m}}^{(0)})$.
2. *Predictor:*
   (i) Set the integration limit $\hat{u}_{\mathrm{m}} = u_{\mathrm{m}}^{(k)}$ and integrate along $\mathcal{R}_1(\boldsymbol{u}_{\mathrm{l}})$ to obtain point $\hat{\boldsymbol{u}}_{\mathrm{m}}$.
   (ii) Set the integration limit $\hat{u}_{\mathrm{m}} = u_{\mathrm{m}}^{(k)}$ and integrate along $\mathcal{R}_2(\boldsymbol{u}_{\mathrm{r}})$ to obtain point $\tilde{\boldsymbol{u}}_{\mathrm{m}}$.
   (iii) Compute eigenvectors $\boldsymbol{r}_1(\hat{\boldsymbol{u}}_{\mathrm{m}})$ and $\boldsymbol{r}_2(\tilde{\boldsymbol{u}}_{\mathrm{m}})$ at the integration endpoints.
3. *Corrector:* new approximation $\boldsymbol{u}_{\mathrm{m}}^{(k+1)}$ is the intersection of two straight lines with orientations $\boldsymbol{r}_1$ and $\boldsymbol{r}_2$ emanating from points $\hat{\boldsymbol{u}}_{\mathrm{m}}$ and $\tilde{\boldsymbol{u}}_{\mathrm{m}}$, respectively.
4. Check convergence:
   IF $||\boldsymbol{u}_{\mathrm{m}}^{(k+1)} - \boldsymbol{u}_{\mathrm{m}}^{(k)}|| < \epsilon$ STOP
   ELSE Set $k \leftarrow k + 1$ and GOTO 2.

Figure 13. Predictor–corrector algorithm for the $\mathcal{R}_1\mathcal{R}_2$ solution.

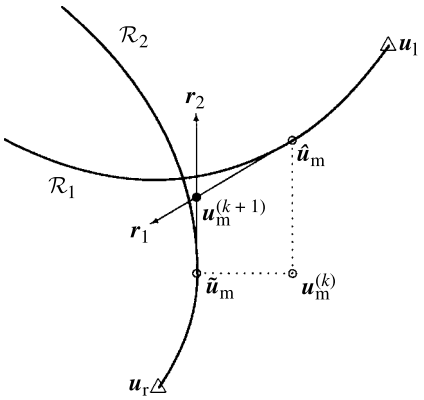

Figure 14. Schematic diagram of the kth iteration of the predictor–corrector procedure for a $\mathcal{R}_1\mathcal{R}_2$ intersection.

As an illustration, we solve the Riemann problem with left state $\boldsymbol{u}_{\mathrm{l}} = (0.5, 0.5)$ and right state $\boldsymbol{u}_{\mathrm{r}} = (0.4, 0.1)$. We use the same relative permeability model and the same viscosities as before. The solution in the ternary diagram is plotted in Figure 3(e). Note that the saturation path never crosses the inflection loci. Figure 12(b) shows the evolution of the error with the number of iterations of the predictor–corrector strategy. Convergence is quadratic because the iterative procedure involves the eigenvectors, which are tangent to the rarefaction curves.

1. Set $k = 0$. Initial guess $\boldsymbol{u}_{\mathrm{m}}^{(0)} = (u_{\mathrm{m}}^{(0)}, v_{\mathrm{m}}^{(0)})$.
2. *Predictor:*
   (i) Set the integration limit $\hat{u}_{\mathrm{m}} = u_{\mathrm{m}}^{(k)}$ and determine the $\mathcal{R}_1\mathcal{S}_1$ curve using the predictor–corrector algorithm in Figure 10, to obtain the post-shock state $\hat{\boldsymbol{u}}_1^*$ and the endpoint $\hat{\boldsymbol{u}}_{\mathrm{m}}$.
   (ii) Integrate along the $\mathcal{R}_2$ curve from point $\hat{u}_{\mathrm{m}}$ towards $\boldsymbol{u}_{\mathrm{r}}$ until $\nu_2(\tilde{\boldsymbol{u}}) = \sigma_2(\tilde{\boldsymbol{u}}; \boldsymbol{u}_{\mathrm{r}})$. Set $\tilde{\boldsymbol{u}}_2^* = \tilde{\boldsymbol{u}}$ at which integration stopped.
   (iii) Set $\hat{v}_2^* = \tilde{v}_2^*$ and solve the $\mathcal{S}_2$ curve passing through the right state $\boldsymbol{u}_{\mathrm{r}}$ to obtain the post-shock state $\hat{\boldsymbol{u}}_2^*$.
3. *Corrector:* new approximation $\boldsymbol{u}_{\mathrm{m}}^{(k+1)}$ is the intersection of curves $\mathcal{S}_1(\hat{\boldsymbol{u}}_1^*)$ and $\mathcal{R}_2(\hat{\boldsymbol{u}}_2^*)$. This is done in a similar fashion to a $\mathcal{R}_1\mathcal{R}_2$ intersection described in Section B.2.
4. Check convergence:

   IF $||\boldsymbol{u}_{\mathrm{m}}^{(k+1)} - \boldsymbol{u}_{\mathrm{m}}^{(k)}|| < \epsilon$ STOP

   ELSE Set $k \leftarrow k + 1$ and GOTO 2.

Figure 15. Predictor–corrector algorithm for the $\mathcal{R}_1\mathcal{S}_1\mathcal{R}_2\mathcal{S}_2$ solution.

B.3. $\mathcal{R}_1\mathcal{S}_1\mathcal{R}_2\mathcal{S}_2$ SOLUTION

We consider the case when both waves are composite rerefaction–shocks. The variables that need to be determined to characterize the solution are: the intermediate constant state $\boldsymbol{u}_{\mathrm{m}}$, the shock speeds σ_1 and σ_2, and the post-shock states $\boldsymbol{u}_1^*$ and $\boldsymbol{u}_2^*$ of each wave. The main difficulty in computing the solution is that both endpoints of the $\mathcal{R}_2$ curve are unknown, so that the initial condition to start integration is not known *a priori*. The predictor–corrector algorithm in Figure 15 has proven very effective.

The solution is admissible if each of the two waves is admissible individually, that is,

$$\mathcal{R}_1\mathcal{S}_1 : \begin{cases} \nu_1 \text{ increases monotonically along } \mathcal{R}_1 \text{ from } \boldsymbol{u}_{\mathrm{l}} \text{ to } \boldsymbol{u}_1^*, \\ \nu_1(\boldsymbol{u}_1^*) = \sigma_1 > \nu_1(\boldsymbol{u}_{\mathrm{m}}), \end{cases}$$

$$\mathcal{R}_2\mathcal{S}_2 : \begin{cases} \nu_2 \text{ increases monotonically along } \mathcal{R}_2 \text{ from } \boldsymbol{u}_{\mathrm{m}} \text{ to } \boldsymbol{u}_2^*, \\ \nu_2(\boldsymbol{u}_2^*) = \sigma_2 > \nu_2(\boldsymbol{u}_{\mathrm{r}}). \end{cases}$$

Using the same relative permeability model and the same viscosities as before, we solve the Riemann problem with left state $\boldsymbol{u}_{\mathrm{l}} = (0.5, 0.5)$ and right state $\boldsymbol{u}_{\mathrm{r}} = (0.05, 0)$. The saturation path in the ternary diagram is shown in Figure 3(i). Each composite wave crosses the inflection locus of the corresponding characteristic family.

References

Al-Futaisi, A. and Patzek, T. W.: 2003, Impact of oil–water drainage and imbibition on subsequent gas injection: A three-phase pore network model, *Phys. Rev. E*, Accepted for publication.

Ancona, F. and Marson, A.: 2001, A note on the Riemann problem for general $n \times n$ conservation laws, *J. Math. Anal. Appl.* **260**, 279–293.

Barenblatt, G. I., Entov, V. M. and Ryzhik, V. M.: 1990, *Theory of Fluid Flows through Natural Rocks*. Kluwer, Dordrecht. Expanded and revised edition of the original in Russian *Dvizhenie zhidkostei i gazov v prirodnykh plastakh*, Nedra Publishers, 1984.

Batycky, R. P., Blunt, M. J. and Thiele, M. R.: 1997, A 3D field-scale streamline-based reservoir simulator, *SPE Reserv. Eng.* **11**(4), 246–254.

Bell, J. B., Trangenstein, J. A. and Shubin, G. R.: 1986, Conservation laws of mixed type describing three-phase flow in porous media, *SIAM J. Appl. Math.* **46**(6), 1000–1017.

Charny, I. A.: 1963, *Subterranean Hydro-Gas Dynamics*, Gostoptekhizdat, Moscow (in Russian).

Chavent, G. and Jaffré, J.: 1986, *Mathematical Models and Finite Elements for Reservoir Simulation*. Elsevier, North-Holland.

Falls, A. H. and Schulte, W. M.: 1992a, Features of three component, three phase displacement in porous media, *SPE Reserv. Eng.* **7**(4), 426–432.

Falls, A. H. and Schulte, W. M.: 1992b, Theory of three component, three phase displacement in porous media, *SPE Reserv. Eng.* **7**(3), 377–384.

Fayers, F. J.: 1987, Extension of Stone's method I and conditions for real characteristics in three-phase flow, in: Proc. of the *SPE Annual Technical Conference and Exhibition*, Dallas, TX (SPE 16965).

Guzmán, R. E. and Fayers, F. J.: 1997a, Mathematical properties of three-phase flow equations, *Soc. Pet. Eng. J.* **2**(3), 291–300.

Guzmán, R. E. and Fayers, F. J.: 1997b, Solution to the three-phase Buckley–Leverett problem, *Soc. Pet. Eng. J.* **2**(3), 301–311.

Guzmán, R. E., Domenico, G., Fayers, F. J., Aziz, K. and Godi, A.: 1994, Three-phase flow in field scale simulations of gas and WAG injections, in: *SPE European Petroleum Conference*, London, UK (Proc. of the SPE 28897).

Helfferich, F. G.: 1981, Theory of multicomponent, multiphase displacement in porous media, *Soc. Pet. Eng. J.* **21**(1), 51–62. *Petrol. Trans.* AIME, 271.

Helfferich, F. and Klein, G.: 1970, *Multicomponent Chromatography*. Marcel Dekker, New York.

Hicks Jr., P. J. and Grader, A. S.: 1996, Simulation of three-phase displacement experiments, *Transp. Porous Media* **24**, 221–245.

Holden, L.: 1990, On the strict hyperbolicity of the Buckley–Leverett equations for three-phase flow in a porous medium, *SIAM J. Appl. Math.* **50**(3), 667–682.

Juanes, R.: 2003, Displacement theory and multiscale numerical modeling of three-phase flow in porous media, PhD Dissertation, University of California at Berkeley.

Juanes, R. and Patzek, T. W.: 2002, Relative permeabilities for strictly hyperbolic models of three-phase flow in porous media, *Transp. Porous Media.*, submitted for publication. Also available as Report LBNL-51442, Lawrence Berkeley National Laboratory.

Keyfitz, B. L. and Shearer, M. (eds): 1990, *Nonlinear Evolution Equations that Change Type*, Springer, New York.

Kyte, J. R., Stanclift Jr., R. J., Stephen Jr., S. C. and Rapoport, L. A.: 1956, Mechanism of water flooding in the presence of free gas. *Petrol. Trans.* AIME **207**, 215–221.

Lax, P. D.: 1957, Hyperbolic system of conservation laws, II, *Commun. Pure Appl. Math.* **10**, 537–566.

LeVeque, R. J.: 1992, *Numerical Methods for Conservation Laws*, 2nd edn, Birkhäuser, Berlin.

Lindquist, W. B. (ed.): 1989, *Current progress in Hyperbolic systems: Riemann Problems and Computations*, American Mathematical Society, Providence, RI.

Liu, T.-P.: 1974, The Riemann problem for general 2×2 conservation laws, *Trans. Amer. Math. Soc.* **199**, 89–112.

Marchesin, D. and Plohr, B. J.: 2001, Wave structure in WAG recovery, *Soc. Pet. Eng. J.* **6**(2), 209–219.

Muskat, M.: 1949, *Physical Principles of Oil Production*, McGraw-Hill, New York.

Oak, M. J., Baker, L. E. and Thomas, D. C.: 1990, Three-phase relative permeability of Berea sandstone, *J. Pet. Technol.* **42**(8), 1054–1061.

Parker, J. C., Lenhard, R. J. and Kuppusamy, T.: 1987, A parametric model for constitutive properties governing multiphase flow in porous media, *Water Resour. Res.* **23**(4), 618–624.

Pope, G. A.: 1980, The application of fractional flow theory to enhanced oil recovery, *Soc. Pet. Eng. J.* **20**(3), 191–205. *Petrol. Trans.* AIME, 269.

Rhee, H.-K., Aris, R. and Amundson, N. R.: 1989, *First-Order Partial Differential Equations, Theory and Application of Hyperbolic Systems of Quasilinear Equations*. Vol. II. Prentice-Hall, Englewood Cliffs, NJ.

Shalimov, B. V.: 1972, Filtration of a three-phase liquid (Buckley–Leverett model) (in Russian). *Izv. Akad. Nauk SSSR, Mekhan. Zhidk. i. Gaza* **7**(1), 39–44. English translation in *Fluid Dyn.*, **7**: 36–40, 1972.

Shearer, M. and Trangenstein, J. A.: 1989, Loss of real characteristics for models of three-phase flow in a porous medium, *Transp. Porous Media* **4**, 499–525.

Stklyanin, Y. I.: 1960, The motion of a mixture of three liquids in a porous medium (in Russian), *Izv. Akad. Nauk SSSR, Otd. Tekh. Nauk, Mekhanika i Mashinostroenie* **2**(5).

Stone, H. L.: 1970, Probability model for estimating three-phase relative permeability, *J. Pet. Technol.* **23**(2), 214–218. *Petrol. Trans.* AIME, 249.

Stone, H. L.: 1973, Estimation of three-phase relative permeability and residual oil data, *J. Can. Petrol. Technol.* **12**(4), 53–61.

Trangenstein, J. A.: 1989, Three-phase flow with gravity, in: W. B. Lindquist (ed.), *Current Progress in Hyperbolic Systems: Riemann Problems and Computations*, American Mathematical Society, Providence, RI, pp. 147–159.

Zauderer, E.: 1983, *Partial Differential Equations of Applied Mathematics*, Wiley, New York.